Biophysical Chemistry 28 (1987) 59–75
Elsevier

BPC 01183

Time-resolved fluorescence anisotropy for systems with lifetime and dynamic heterogeneity

Richard D. Ludescher *, Linda Peting **, Suzanne Hudson and Bruce Hudson

Department of Chemistry and Institute of Molecular Biology, University of Oregon, Eugene, OR 97403, U.S.A.

Received 30 March 1987
Revised manuscript received 23 June 1987
Accepted 24 June 1987

Fluorescence decay; Anisotropy decay

The time dependence of the fluorescence anisotropy expected when a fluorophore exists in distinct environments having different fluorescence decay and motional behavior is illustrated by simulation calculations. A wide range of behavior is observed. The analysis of such decays in terms of the underlying physical parameters is also illustrated and discussed. In particular, the analysis of 'associated' heterogeneous behavior using a homogeneous environment model with complex motional behavior is evaluated. It is argued that anisotropy decays that exhibit a high initial anisotropy and that rise at long times must be due to a heterogeneous environment. Anisotropic rotor diffusion cannot give rise to behavior of this type. A similar conclusion is reached for anisotropies that exhibit downward curvature. On the other hand, anisotropy decays that are monotonically decreasing and have a positive second derivative at all times cannot be analyzed in a unique fashion and therefore an ambiguity exists in the interpretation of such data in terms of motional behavior.

1. Introduction

The use of time-resolved fluorescence anisotropy measurements in studies of molecular dynamics is enjoying increased interest because of instrumental and theoretical advances. Modern developments in laser technology and electronics permit subnanosecond measurements on a routine basis with considerable reliability [1]. Recent theoretical studies have emphasized formalisms for the analysis of anisotropy decays that apply to specific biophysical problem [2–8] or provide very general formulations [9,10]. Simulations of biopolymer dynamics at the atomic level can be used to calculate the expected anisotropy behavior directly [11,12]. A comparison of such calculations with experiment represents a test of these calculation methods.

Most treatments of fluorescence anisotropy decay have been concerned with the connection between the rotational dynamics of the emission dipole of a molecule and the anisotropy decay for an idealized fluorescence experiment with a homogeneous fluorophore environment. Real fluorescence data, however, are usually more complicated. In particular, fluorophores often exhibit nonexponential decay that may be described in terms of several lifetimes. This may be due to the presence of the fluorophore in distinct environments that interconvert slowly. We have examined the anisotropy decay expected for samples containing a mixture of fluorophore environments [1,13]. The equations describing this situation are well known [13–19] but the potential variety of

Correspondence address: B.S. Hudson, Department of Chemistry and Institute of Molecular Biology, University of Oregon, Eugene, OR 97403, U.S.A.
* Present address: Department of Chemistry, The Wichita State University, Wichita, KS 67208, U.S.A.
** Present address: California Institute of Technology, Pasadena, CA 91125, U.S.A.

the resulting anisotropy decays does not seem to have been illustrated. Furthermore, the question of the unique interpretation of such data does not seem to have been addressed. It is important to know to what extent the true physical parameters of a system can be extracted from an observed set of data and to evaluate the possibility that more than one interpretation is possible.

If distinct species in a sample have different fluorescence decay behavior and a corresponding variation in motional behavior, the curvature in the measured anisotropy decay may have little or no relation to molecular motion. Our interest in this problem was prompted by the observation of unusual anisotropy behavior of fluorophores in lipid bilayer samples [1,18,19] and lipid/protein systems [1,7,18] (see fig. 1). Other workers have reported anisotropy behavior similar to that described here [16,20–25]. The simulations presented here should provide a starting point for the analysis of a variety of specific cases.

The physical picture that underlies these simulations is simple. When a heterogeneous sample contains several fluorescing species, the emission at short times is due to all of the lifetime components. At long times, however, the observed fluorescence is due only to the longest-lifetime component. The observed anisotropy is thus a weighted average of the behavior of all components at short times, but at sufficiently long times is due solely to the rotational diffusion of the species with the longest lifetime. A simple example will illustrate this point. A sample that contains a fluorophore free in solution and bound to a biopolymer will have a complicated anisotropy decay due to the fact that the free fluorophore will rotate much faster than the bound probe. If the lifetimes for the two probes environments are the same, then the measured anisotropy is just the sum of that for the free and bound probe. If, however, the two states of the fluorophore have different lifetimes (a common situation), then, depending on whether the long-lifetime species is bound or free in solution, the long-time anisotropy will reflect the rotation of either the protein or the unbound fluorophore. The time-dependent increase in the contribution of the long-lifetime component may cause the curve to rise or fall at long times. Therefore, the shape of the measured anisotropy decay may bear no direct relationship to motional behavior per se.

In many other cases the multiple-lifetime (or, in general, nonexponential) behavior observed for the decay of the total fluorescence may have no

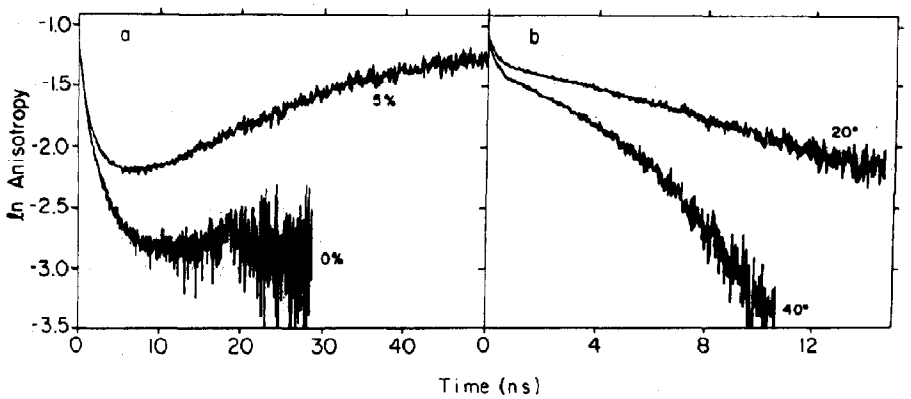

Fig. 1. Experimental examples of anomalous anisotropy decays. The anisotropy is calculated from the undeconvoluted parallel and perpendicular transients taking the peak of the machine response function as time zero. (a) *trans*-Parinaric acid in egg phosphatidylcholine/cholesterol vesicles. The cholesterol content is 0 and 5 mol% as indicated. Excitation is at 300 nm with emission monitored at 430 nm through a broad-band filter. See refs. 1 and 18 for further details. (b) Anisotropy decay of the fluorescence of the single tryptophan of phospholipase A_2 in a micellar complex with the nonhydrolyzable substrate analog *n*-hexadecylphosphocholine at the indicated temperatures. See refs. 1, 13 and 18 for details.

obvious connection with distinct chemical 'species' having distinct dynamic behavior. In these cases, the correlation between lifetime 'components' and anisotropy behavior becomes unclear. The lifetime heterogeneity of tryptophan in proteins is an example of such a problematic case [1,13,26–33]. The complex photophysics of the indole chromophore [27–31] makes the excited-state decay behavior of tryptophan an especially complicated problem. The real situation for many biopolymer probe molecules, moreover, may be that the rates of excited-state decay (the inverse lifetimes) are continuously distributed [34]. These distributions may be unimodal or multimodal. The factors that determine the distribution will depend on the particular fluorophore but are generally related to local fluctuations in polarizability, due to density fluctuations, or electric field, due to dipole fluctuations. For biopolymer environments, some of these fluctuations will persist for times that are long compared to fluorescence lifetimes [10,35–38]. The same factors that determine excited-state decay rates are also likely to influence the rotational diffusion of the fluorophore. If this turns out to be the case, the anisotropy decay can be properly understood only in terms of a model that associates each lifetime species with particular dynamic behavior.

The specific model we treat here is applicable when the following conditions are met. First, there are two distinct populations of fluorophores with different lifetimes. These may be different molecules or the same molecule in different environments. Second, these populations do not interconvert on the time scale of the fluorescence lifetime. Third, the different populations have distinct dynamic behavior. We specifically exclude from this model cases in which two populations of fluorophores interconvert during the lifetime of the excited state or cases in which the initially excited molecules undergo a reaction prior to emitting radiation. A model has recently been proposed [38] based on coupling between solvent relaxation around a polar excited state and the rate of fluorophore depolarization. This interesting analysis specifically differs from our treatment by including solvent relaxation that occurs during the fluorescence lifetime.

2. Mathematical formulation

2.1. Time-dependent weighting factors

A heterogeneous population of fluorophores, either the same chromophore in different environments or different chromophores, generally has a complicated form for the total fluorescence decay. Each class of fluorophores has its own decay law, $I_i(t)$, and the total decay is the sum of the component decays:

$$I(t) = \sum_{i=1}^{n} a_i I_i(t) \tag{1}$$

where n is the total number of distinct chemical species in the mixture and $\sum_{i=1}^{n} a_i = 1$. If we consider the fluorescence of a sample following a δ-function excitation, the fraction of the total light emitted at any time t by species, i, $f_i(t)$, is the ratio of the decay law for that species to the decay law for the entire system:

$$f_i(t) = a_i I_i(t)/I(t). \tag{2}$$

It follows that $\sum_{i=1}^{n} f_i(t) = 1$. The fractional contribution of species i to the total light intensity is thus a function of time. We can formulate an analytical function for eq. 2 by noting that, in many cases, $I_i(t)$, the decay behavior for a particular species, is a single exponential. With this assumption, we associate a fluorescence lifetime component with a particular species. This is not completely general but does serve to illustrate the major effect of interest here. We then have

$$f_i(t) = a_i \exp(-t/\tau_i) / \sum_{j=1}^{n} a_j \exp(-t/\tau_j)$$

$$= a_i / \left\{ a_i + \sum_{\substack{j=1 \\ j \sim i}}^{n} a_j \exp\left[-t\left(1/\tau_j - 1/\tau_i\right)\right] \right\} \tag{3}$$

At time zero, $f_i(0) = a_i$ for all species. The weighting factors a_i are given by the relative absorption of that species (proportional to the mole fraction of that species for equal extinction coefficients at the excitation wavelength) times the radiative rate constant divided by the sum of such

products. (We assume that each species has the same emission spectrum.) At later times the various $f_i(t)$ functions time-evolve according to the summation term in the denominator of eq. 3. If the components are ordered from shortest- to longest-lifetime species, then all $f_i(t)$, except $f_n(t)$, have at least one term in the denominator of the last expression where $\tau_j > \tau_i$. This results in a positive exponential term in the sum, and $f_i(t)$ will decay to zero as t goes to infinity ($t \gg \tau_i$). The fraction of the shortest-lifetime species, $f_1(t)$, decays monotonically to zero; the fractions of the other species may initially increase before decaying to zero. In contrast, the fraction of the longest-lifetime species, $f_n(t)$, goes to unity at long times. Examples of this behavior for a system with two lifetime species are shown in fig. 2 for three different values of the ratio τ_2/τ_1. The rate at which the long-lifetime species becomes the major fluorescence component increases as τ_2/τ_1 increases.

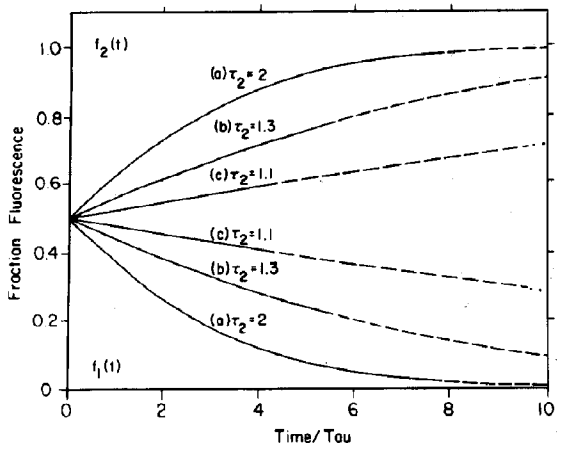

Fig. 2. Time dependence of the fractional fluorescence of the individual species in a heterogeneous sample. The fractional fluorescence, $f_1(t)$ and $f_2(t)$, for a sample with two fluorescent components of equal amplitude is plotted for three different values of the long-lifetime component, τ_2. The value of τ_1 is 1.0 in all three cases. The values of τ_2 are 2.0 (curves a), 1.3 (curves b) and 1.1 (curves c). $f_2(t)$ corresponds to the upper and $f_1(t)$ to the lower set of curves. The curves are shown as dashed lines for times beyond the point where the total fluorescence intensity has fallen to 1% of the peak value and as dotted lines beyond the point where the intensity has fallen to 0.1% of the peak value.

2.2. *Influence of weighting factors on anisotropy decay*

The experimental anisotropy decay of a system following a δ-function excitation with vertically polarized light is:

$$r(t) = [I_V(t) - I_H(t)]/[I_V(t) + 2I_H(t)] \equiv D(t)/I(t) \quad (4)$$

For a heterogeneous system, $r(t)$ is a linear combination of the anisotropy decays of each lifetime species in the mixture:

$$r(t) = \sum_{i=1}^{n} f_i(t) r_i(t) \quad (5)$$

where $f_i(t)$ is given by eq. 2 and $r_i(t)$ is the anisotropy decay of species i. If there is no dependence of the anisotropy decay on the factors determining the fluorescence decay of a species, $r_i(t) = r(t)$ for all species and the experimental anisotropy, $r(t)$, is equal to the molecular anisotropy, $r(t)$,

$$r(t) = r(t) \sum_{i=1}^{n} f_i(t) = r(t)$$

The steady-state anisotropy, $\langle r \rangle$, obtained under conditions of continuous illumination is given by

$$\langle r \rangle = (I_V - I_H)/(I_V + 2I_H).$$

$\langle r \rangle$ is related to the integral of the time-dependent expression for the measured anisotropy

$$\langle r \rangle = \int_0^\infty r(t) I(t)\, dt / \int_0^\infty I(t)\, dt \quad (6)$$

If we substitute eqs. 1, 2, and 5 into this equation, we can calculate $\langle r \rangle$ for the model under discussion. The result is Weber's Law for addition of polarization couched in terms of anisotropy.

$$\langle r \rangle = \sum_{i=1}^{n} g_i \langle r_i \rangle \quad (7)$$

Here g_i is the fraction of the total fluorescence due to species i ($g_i = a_i \tau_i$ for the case of single-exponential decay for each species).

2.3. Form of the component anisotropy decays used in r(t) simulations

The general expression for $r_i(t)$ may involve five or more exponentials [8,10,25]. The determination of this number of components is unrealistic in actual application. It has been demonstrated for the case of rotational diffusion of an ellipsoid of revolution that two pairs of these terms are practically identical so that the sum is well represented by three terms [39]. We will consider the case of a fluorophore that is free to rotate through a limited angular range attached to a large particle that undergoes isotropic rotational diffusion. This case has been treated by Kinosita et al. [4] and Lipari and Szabo [9] and results in a decay that is well approximated by two exponential terms:

$$r_i(t) = r(0)\left[\alpha_i \exp(-t/\phi_i) + (1-\alpha_i)\right] \times \exp(-t/\phi_p) \quad (8)$$

where ϕ_i is the rotational correlation time of the fast internal motion for species i, α_i the amplitude of this motion and ϕ_p the decay time for overall particle tumbling. In this expression we have made the assumption that $r_i(0) = r(0)$ for all i. This means that the lifetime heterogeneity is presumed to result from a single molecular species experiencing environments that differ only in their radiationless decay rate. This is often, but not always, the case.

The simulations to be presented all assume a value of $r(0) = 2/5$, the maximum possible, corresponding to colinearity of the absorption and emission transition dipoles. This choice is made partly for simplicity (any other initial value results in a simple multiplication of the anisotropy by a constant). Also, the value of $r(0) = 2/5$ corresponds to the observed value for parinaric acid, a fluorescent probe used in many of our experiments [1,7,13,18,19,40,41]. Another reason for this choice is that if $r(0)$ is small (particularly if it is negative), it is possible to observe anisotropy curves with some similarity to those presented here for a physically very different reason, namely, anisotropic rotational diffusion [42,43]. In particular, this can give rise to anisotropies that increase with time. However, such behavior requires noncolinearity of the absorption and emission transition dipoles and thus an initial value of r substantially lower than 0.4.

In this model for $r_i(t)$, the values of ϕ_p determine the decay behavior at long times. The realistic time scale for actual measurements is limited to a few times τ_2, the longer fluorescence lifetime. If $\phi_p \gg \tau_2$, then $r(t)$ decays to a constant, $r(\infty)_2 = [(1-\alpha_2)r(0)]$. This is the case for fluorophores in membranes, vesicles, or other large macromolecular complexes where particle tumbling is slow on the fluorescence time scale. If ϕ_p is comparable to τ_2, then the decay is isotropic at long times and $r(t)$ decays to zero. This is the case for fluorophores associated with proteins, detergent micelles, or other small macromolecular complexes.

2.4. Experimental simulation by convolution and subsequent analysis

In order to determine the extent to which experimental anisotropy decay curves for heterogeneous environments can be analyzed to give unique information, many of these cases were used to simulate actual data. This was done by convoluting the computed I_V and I_H transients with an actual instrument response function (full-width at half-maximum of 150 ps) and adding noise corresponding to 10^6 counts in the peak channel. This was done with a Gaussian random number generator. The resulting 'data sets' were then analyzed using nonlinear numerical deconvolution procedures based on the Marquardt algorithm. The simulated vertical and horizontal experimental results were analyzed simultaneously using all of the parameters of the fluorescence and anisotropy decay as adjustable quantities [44]. Estimates of the statistical reliability of the adjusted parameters are made using standard methods [45].

3. Results

The presentation of the types of unusual behavior that can occur with this model will be done on a case-by-case basis in which we examine the

types of $r(t)$ curves that can result from using successively more complicated expressions for $r_i(t)$. In case I the anisotropy decays, $r_i(t)$, for each species are described by a single exponential ($\alpha_i = 0$ or 1 for each i in eq. 8). Variations in the values of the lifetimes (τ_i) and the lifetime amplitudes (a_i) will provide examples of most of the kinds of anomalies that can arise in experimental $r(t)$ decays. Case II describes each $r_i(t)$ as an exponential decay to a constant ($\alpha_i < 1$ and $\phi_p \gg \tau_2$ in eq. 8). This introduces one new parameter, α_i, that can have important effects on the sum $r(t)$ curves. In case III the particle rotational correlation time, ϕ_p, is comparable to τ_2 and $r_i(t)$ is a double-exponential decay for each species.

This procedure will provide a kind of natural history of the types of behavior that can be expected to occur in measured $r(t)$ decays of fluorophores in complicated biophysical systems. In section 4, we will discuss how (and to what extent) this information can be used to determine the actual molecular anisotropy behavior, the $r_i(t)$ decays, from the measured $r(t)$ decays.

3.1. Case I: Single correlation time for each component anisotropy decay

If we set $\alpha_i = 1$ and $\phi_p \gg \phi_i$ in eq. 8 then, using eqs. 3 and 5, the total $r(t)$ decay has the form:

$$r(t) = r(0)\left[f_1(t)\exp(-t/\phi_1) + f_2(t)\exp(-t/\phi_2)\right] \quad (9)$$

($f_i(t) = a_i \exp(-t/\tau_i)/I(t)$). In this and all subsequent simulations, species 2 is the long-lifetime component. This is the simplest case for a two-component system.

Because $\alpha_i = 1$ and ϕ_p is very large (compared to τ_2), the values of ϕ_1 and ϕ_2 correspond to correlation times for unrestricted isotropic motions of two fluorophore species in different environments. Since the motion is isotropic, there is no way to distinguish this motion from overall particle reorientation. Setting $\alpha_i = 0$ for both species results in the same functional form with ϕ_i replaced by an overall particle correlation time, ϕ_p.

The curves that result from eq. 9 (fig. 3) can be organized into two classes: 'decelerating' curves in which the $r(t)$ decays rise at intermediate times and 'accelerating' curves in which the decays curve downward at long times. The former class is due to the presence of a long-lifetime component with a longer rotational correlation time and the latter class to a long-lifetime component with a shorter correlation time.

3.1.1. Case I with $\phi_2 > \phi_1$

The class of decelerating anisotropy decays is illustrated by the family of curves in fig. 3a. For this simulation we have set $\tau_1 = 1.0$, $\tau_2 = 2.0$, $\phi_1 = 0.5$ and $\phi_2 = 5.0$ and plotted the natural logarithm of $r(t)$ vs (time/τ_1) for several values of a_1, the amplitude of the short-lifetime component. The use of dimensionless time variables makes explicit that it is the ratio of the relevant parameters that is important and not their absolute value. The curved lines in fig. 3a range between two straight lines that are plots of the limiting behavior of the short-lifetime species ($\phi_1 = 0.5$) and long-lifetime species ($\phi_2 = 5.0$), i.e., $a_1 = 1$ or $a_2 = 1$. The most striking feature of these simulations is the degree of upward curvature in curves with $a_2 < 0.15$ ($a_2 = 1 - a_1$). We find that this is characteristic of all of the simulations: the curvature due to adding $r(t)$ decays is most pronounced when the long-lifetime component is less than 10–15% of the total decay.

The decays in fig. 3a (and in all other figures) are shown on a time scale of $10\tau_1$. Collection of data on such a long time scale may not be possible (or desirable) in practice. As illustrated by decays with $a_2 < 0.1$, the lack of data at long times may have the result that the slope of $\log[r(t)]$ has no relation to the rotational correlation time of any component in the mixture. In these cases, the upward curvature indicates the heterogeneous nature of the sample. As another example, the curve in fig. 3a corresponding to $a_1 = 0.8$ may be interpreted as decay to a nonzero constant if sufficient data at long times are not available. Since this type of behavior is physically reasonable, this $r(t)$ behavior may be improperly interpreted.

The degree of upward curvature in $r(t)$ is influenced by the ratio ϕ_2/ϕ_1. If ϕ_2 decreases, the component decay curves $r_1(t)$ and $r_2(t)$ approach

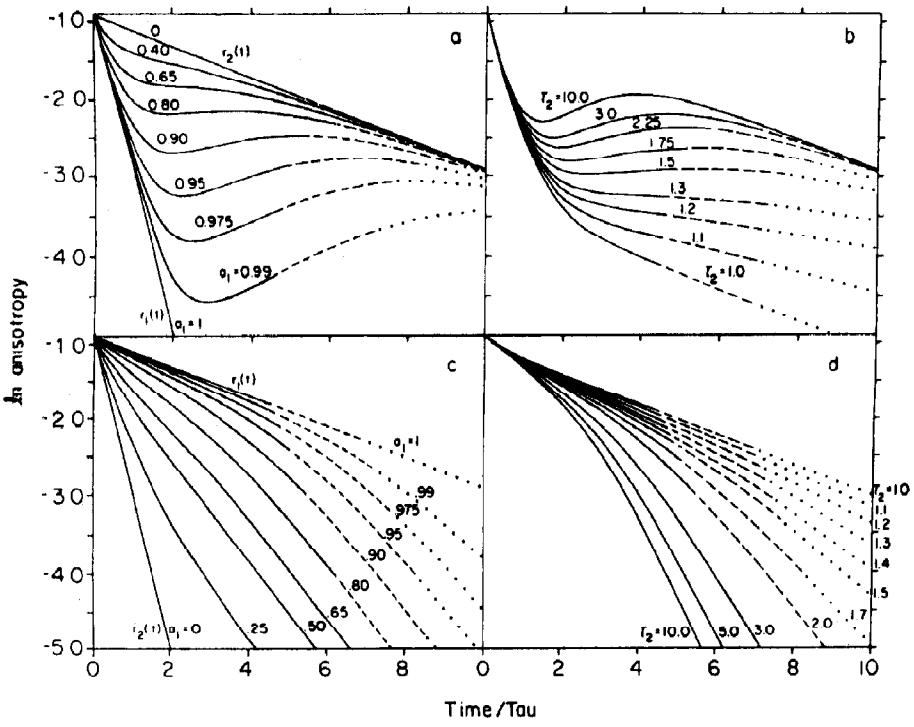

Fig. 3. Simulated anisotropy decays for case I calculated according to eq. 9. (a) The curves differ in the value of a_1, the amplitude of the short-lifetime component, with $\tau_1 = 1.0$, $\tau_2 = 2.0$, $\phi_1 = 0.5$ and $\phi_2 = 5.0$. The values of a_1 (lower to upper curves) are 1.0, 0.99, 0.975, 0.95, 0.9, 0.8, 0.65, 0.4 and 0. (b) The curves differ in the value of τ_2, the long lifetime, with $\tau_1 = 1.0$, $a_1 = 0.9$, $\phi_1 = 0.5$ and $\phi_2 = 5.0$. The values of τ_2 (lower to upper curves) are 1.0, 1.1, 1.2, 1.3, 1.5, 1.75, 2.25, 3.0 and 10. (c) The curves differ in the value of a_1, the amplitude of the short-lifetime component, with $\tau_1 = 1.0$, $\tau_2 = 2.0$, $\phi_1 = 5.0$ and $\phi_2 = 0.5$. The values of a_1 (upper to lower curves) are 1.0, 0.99, 0.975, 0.95, 0.9, 0.8, 0.65, 0.5, 0.25 and 0. (d) The curves differ in the value of τ_2, the long lifetime, and are calculated with $\tau_1 = 1.0$, $a_1 = 0.9$, $\phi_1 = 5.0$ and $\phi_2 = 0.5$. The value of τ_2 (upper to lower curves) are 1.0, 1.1, 1.2, 1.3, 1.4, 1.5, 1.7, 2.0, 3.0, 5.0 and 10. The curves are drawn, as in fig. 2, as dashed lines beyond the time where the total fluorescence intensity has dropped to 1% and as dotted lines beyond 0.1%.

one another and the effect of adding a larger fraction of $r_2(t)$ to the long-time behavior of the sum $r(t)$ decreases. As a result, the curvature in the intermediate curves $(0 < a_1 < 1)$ also decreases.

The magnitude of the rise in $r(t)$ at long times is also a function of the relative values of τ_1 and τ_2. This is illustrated in fig. 3b. ϕ_1 and ϕ_2 have the same values as in fig. 3a (0.5 and 5.0) and we have set $a_2 = 0.1$ to display a large effect due to changes in τ_2. The lowest curve has $\tau_1 = \tau_2 = 1.0$ and illustrates the decay in the absence of lifetime effects: the measured curve is an exact reflection of the component decays. The other curves (from bottom to top) illustrate what happens when τ_2 increases. At τ_2/τ_1 ratios greater than 1.5, these $r(t)$ decays have a local minimum and rise at long times to coincide eventually with the decay due to the long-lifetime species. When τ_2/τ_1 is less than 1.5, however, the effect of environmental heterogeneity is more subtle. There is no rise at long times to indicate anomalous behavior. These curves all eventually converge at long times to the curve for $\phi_2 = 5.0$, but the measured decay over the plotted time scale has a smaller slope. Since it is often not possible to collect data up to long enough times to detect the anomalous effect in these cases, the result is that the apparent long rotational correlation time is larger than the actual value.

3.1.2. Case I with $\phi_1 > \phi_2$

Anisotropy decays with ϕ_1 larger than ϕ_2 display downward curvature at long times ($\tau_2 > \tau_1$ by definition). The slope of a plot of $\log[r(t)]$ becomes more negative as time increases and thus the curves appear to accelerate at long times. This is illustrated by fig. 3c, a plot of $\log[r(t)]$ for a family of curves generated by varying a_1, the short-lifetime amplitude. Fig. 3c uses the same values of the lifetime and anisotropy terms as the curves in fig. 3a and b except that ϕ_1 and ϕ_2 have been interchanged: the short-lifetime species (component 1) now has the longer rotational correlation time. The downward curvature seen in these curves is more subtle than the dramatic rises at long times seen above. As in fig. 3a, the amount of curvature is more pronounced when the long-lifetime species is a small fraction of the fluorophores, $a_2 \leq 0.15$. When $a_2 > 0.5$ the decays do not show noticeable downward curvature.

The effect of lifetime heterogeneity is best illustrated by varying the magnitude of the long lifetime. Fig. 3d is a plot of a family of $\log[r(t)]$ curves generated with different values of τ_2 using the same parameters as fig. 3b except that in this case the long-lifetime component has the shorter correlation time. The degree of curvature increases as τ_2/τ_1 increases (curves from top to bottom). At τ_2/τ_1 ratios greater than 1.3 the downward curvature is obvious. At ratios less than 1.3, however, the curvature is subtle and may be incorrectly interpreted as a smaller value of the long rotational correlation time.

3.2. Case II: Exponential decay to a constant

If we set $\alpha_i < 1$ and $\phi_p \gg \phi_i$ in eq. 8 then, using eqs. 3 and 5, $r(t)$ becomes:

$$r(t) = r(0)\{f_1(t)[\alpha_1 \exp(-t/\phi_1) + (1-\alpha_1)] + f_2(t)[\alpha_2 \exp(-t/\phi_2) + (1-\alpha_2)]\} \quad (10)$$

When $\alpha_1 < 1$, the component anisotropy decays to a nonzero, constant value called r_∞; in our formalism, $r_{\infty i}$ is equal to $[(1-\alpha_i)r(0)]$. Including a constant term in the component anisotropy introduces another possibility for curvature in $r(t)$. If the r_∞ values are not equal, the time dependence of the weighting factors can introduce upward curvature ($\alpha_1 > \alpha_2$) or downward curvature ($\alpha_1 < \alpha_2$) in $r(t)$. We will examine the specifics of these cases in turn.

3.2.1. Case II with $r_{\infty 1} = r_{\infty 2}$

When $\alpha_1 = \alpha_2$, the asymptotic values $r_{\infty 1}$ and $r_{\infty 2}$ become equal. In this case, the results of changes in a_i or τ_2 are very similar to the effects shown in fig. 3 for $\alpha_1 = \alpha_2 = 0$. The only difference is that the anisotropy now decays to a nonzero constant value. Upward curvature occurs when the long-lifetime component decays slowly ($\phi_2 > \phi_1$) and downward curvature occurs when it decays quickly ($\phi_2 < \phi_1$). The generalizations concerning this case are the same as for case I: the maximum curvature occurs when $a_2 < 0.15$, and the curvature increases as the ratio τ_2/τ_1 increases; when $\phi_2 > \phi_1$, the upward curvature increases as ϕ_2/ϕ_1 increases and, when $\phi_2 < \phi_1$, the downward curvature increases as the ratio ϕ_2/ϕ_1 decreases.

3.2.2. Case II with $\alpha_1 > \alpha_2$ ($r_{\infty 2} > r_{\infty 1}$)

The dramatic effects on the measured anisotropy of a long-lifetime species with a high r_∞ are illustrated in fig. 4a. The lowest curve is the component decay of a species with a very rapid, large-amplitude internal motion ($\phi_1 = 0.5$ and $\alpha_1 = 0.75$). The top curve is the component decay of a species exhibiting rapid internal motion with a higher limiting anisotropy ($\phi_2 = 0.5$ and $\alpha_2 = 0.25$). The other curves are linear combinations of these decays using different values of a_1 for the case where the high-anisotropy species has a lifetime twice that of the low-anisotropy species. In no decay does $r(t)$ accurately reflect the dynamics of the components after about one unit of time. As in case I ($\alpha_i = 1.0$), the largest upward curvature is found when the long-lifetime component is a small fraction of the fluorophores ($a_2 < 0.15$). The curves in fig. 4a correspond to $r_{\infty 1} = 0.1$ and $r_{\infty 2} = 0.3$. This large difference in the limiting anisotropies emphasizes the rise at long times. The effects of different values of r_∞ on $r(t)$ are not difficult to anticipate: the magnitude of the rise at long times increases as the difference $(r_{\infty 2} - r_{\infty 1})$ increases.

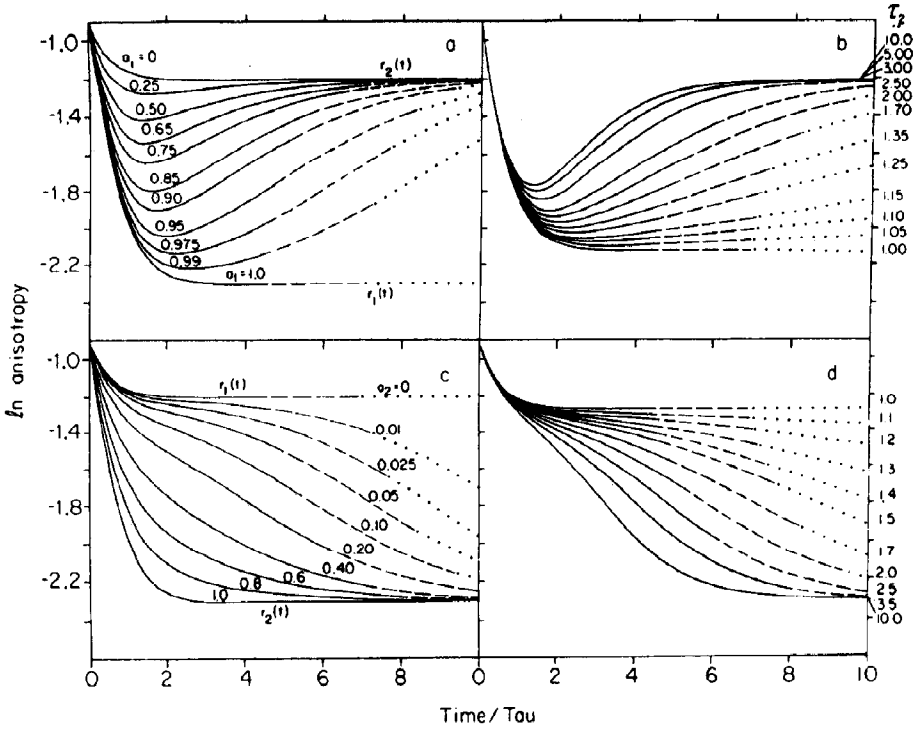

Fig. 4. Simulated anisotropy decays for case II calculated from eq. 10. (a) The curves differ in the value of a_1, the amplitude of the short-lifetime component, and are calculated with $\tau_1 = 1.0$, $\tau_2 = 2.0$, $\phi_1 = \phi_2 = 0.5$, $\alpha_1 = 0.75$ and $\alpha_2 = 0.25$. The values of a_1 (lower to upper curves) are 1.0, 0.99. 0.975, 0.95, 0.9, 0.85, 0.75, 0.65, 0.5, 0.25 and 0. (b) The curves differ in the value of τ_2, the long lifetime, and are calculated with $\tau_1 = 1.0$, $a_1 = 0.9$, $\phi_1 = \phi_2 = 0.5$, $\alpha_1 = 0.75$ and $\alpha_2 = 0.25$. The values of τ_2 (lower to upper curves) are 1.0, 1.05, 1.1, 1.15, 1.25, 1.35, 1.7, 2.0, 2.5, 3.0, 5.0 and 10. (c) The curves differ in the value of a_1, the amplitude of the short-lifetime component, with $\tau_1 = 1.0$, $\tau_2 = 2.0$, $\phi_1 = \phi_2 = 0.5$, $\alpha_1 = 0.25$ and $\alpha_2 = 0.75$. The values of a_1 (lower to upper curves) are 0, 0.2, 0.4, 0.6, 0.8, 0.9, 0.95, 0.975, 0.99 and 1.0. (d) The curves differ in the value τ_2, the long-lifetime component, with $\tau_1 = 1.0$, $a_1 = 0.9$, $\phi_1 = \phi_2 = 0.5$, $\alpha_1 = 0.25$ and $\alpha_2 = 0.75$. The values of τ_2 (upper to lower curves) are 1.0, 1.1, 1.2, 1.3, 1.4, 1.5, 1.7, 2.0, 2.5, 3.5 and 10.0. The lines are drawn as for figs. 2 and 3.

The specific details of the curvature in $r(t)$ at long times are related to the magnitude of the rotational correlation time of the components. If the ϕ values are small ($\phi_i < \tau_1$), $r(t)$ decays quickly to a minimum that is a weighted average of $r_{\infty 1}$ and $r_{\infty 2}$; however, if the correlation times are long, there will be no local minimum in the curve and no increase at long times, merely a gradual decay of r_∞. These situations are illustrated in fig. 5a where $r_{\infty 1} = 0.1$ and $r_{\infty 2} = 0.3$ and the curves differ only in the magnitude of ϕ_i ($\phi_1 = \phi_2$ for all curves). It is worth noting that when the ϕ values are very small, the sum $r(t)$ curve rises over all but the earliest part of the decay.

The magnitude of the increase in $r(t)$ is also a function of the relative magnitude of τ_2 and τ_1. When τ_2/τ_2 is less than about 1.5, the increase is very gradual and appears linear on a logarithmic scale. When $\tau_2/\tau_1 > 3.0$, however, the increase is abrupt. This is illustrated in fig. 4b for component decays that have a short rotational correlation time. The lowest curve in fig. 4b has $\tau_1 = \tau_2$ and therefore represents the actual ensemble average dynamic behavior of the components. As τ_2/τ_1 increases (bottom to top), the upward curvature increases and the lifetime artifact becomes more obvious. Again, the curves do not reflect the component decays except at early times.

3.2.3. *Case II with* $\alpha_1 < \alpha_2$ ($r_{\infty 2} < r_{\infty 1}$)

When $\alpha_1 < \alpha_2$, the limiting anisotropy for the short-lifetime species, $r_{\infty 1}$, is larger than the value

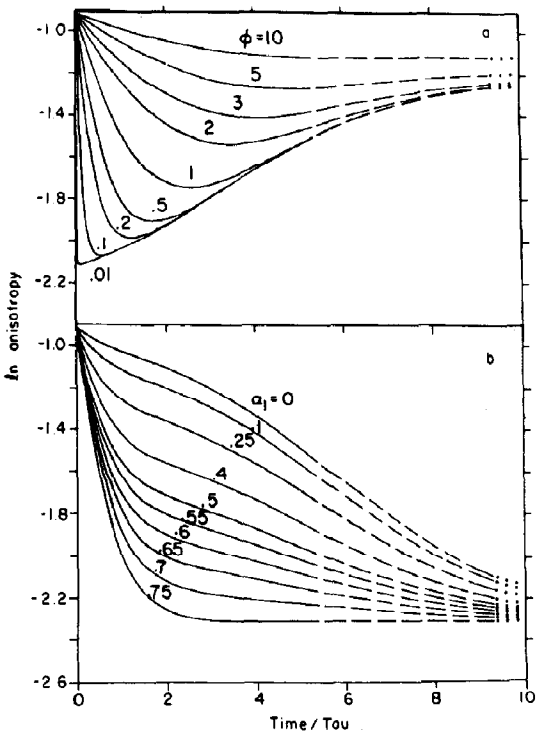

Fig. 5. Simulated anisotropy decays for case II calculated according to eq. 10. (a) The curves differ in the value of ϕ, the rotational correlation time of the component decays (in these curves $\phi_1 = \phi_2$), with $\tau_1 = 1.0$, $\tau_2 = 2.0$, $a_1 = 0.9$, $\alpha_1 = 0.75$ and $\alpha_2 = 0.25$. The values of ϕ (lower to upper curves) are 0.01, 0.1, 0.2, 0.5, 1.0, 2.0, 3.0, 5.0 and 10. (b) The curves differ in the value of α_1, the amplitude of the internal motion of the short-lifetime component, with $\tau_1 = 1.0$, $\tau_2 = 2.0$, $a_1 = 0.9$, $\phi_1 = \phi_2 = 0.5$ and $\alpha_2 = 0.75$. The values of α_1 (lower to upper curves) are 0.75, 0.7, 0.65, 0.6, 0.55, 0.5, 0.4, 0.25, 0.1 and 0. The lines are drawn as for fig. 2.

for the long-lifetime species and the anisotropy may curve downward at long times. When the amplitude of the long-lifetime species, a_2, is less than 0.1, the downward curvature can be quite precipitous. This is illustrated in the upper curves of fig. 4c where the $r(t)$ decays differ only in the fraction of the two species. If $a_2 > 0.1$ (lower curves of fig. 4c), or if the data are not collected up to sufficiently long times, the anisotropy decay appears to have an additional decay mode. This effect is most pronounced when α_1 is only slightly smaller than α_2. This is illustrated in fig. 5b in which the fraction of the long-lifetime component is small ($a_2 = 0.1$) and the plotted curves differ only in the magnitude of α_1 with a fixed value of $\alpha_2 = 0.75$ ($r_{\infty 2} = 0.1$). In the lowest curve ($\alpha_1 = \alpha_2$), there is no effect of the heterogeneity on the $r(t)$ decay ($r_1(t) = r_2(t)$). This is the only curve in fig. 5b that accurately represents the ensemble average molecular dynamics. The lower curves which have $r_{\infty 1} \approx r_{\infty 2}$ appear to represent straightforward double-exponential decays to a constant; the longer decay component, however, is a consequence of the sample heterogeneity. Only at larger values of $r_{\infty 1}$ is the downward curvature at long times revealed, indicating the origin of the long time decay.

Small differences in the lifetimes of the fluorescent components can also lead to spurious anisotropy decays that do not show obvious anomalies. Fig. 4d illustrates the behavior of $\log[r(t)]$ for various values of τ_2. The upper curve is the case without lifetime effects ($\tau_1 = \tau_2$). The curve is a single-exponential decay to a constant. The remaining curves are generated by gradually increasing τ_2 with $r_{\infty 2} < r_{\infty 1}$ to induce downward curvature in $r(t)$. At τ_2/τ_1 ratios very close to 1 (the upper 3–4 curves in fig. 4d), $r(t)$ appears to have a decay mode with a long correlation time. Only at larger values of τ_2 does the downward curvature characteristic of lifetime heterogeneity appear, and then only at long times (greater than $5\tau_1$).

3.3. Case III: Double-exponential decay

When the macromolecule that carries a fluorophore is small enough that the rotational correlation time of the particle, ϕ_p, is of the same order of magnitude as τ_2, all the terms in eq. 8 must be included in $r_i(t)$. The anisotropy for the system becomes:

$$r(t) = r(0)\{f_1(t)[\alpha_1 \exp(-t/\phi_1) + (1-\alpha_1)] + f_2(t)[\alpha_2 \exp(-t/\phi_2) + (1-\alpha_2)]\} \times \exp(-t/\phi_p) \quad (11)$$

(We have assumed, for simplicity, that only one spherical macromolecule is involved so that ϕ_p is the same for both species.) Introducing this whole-particle rotation into the expression for $r_i(t)$ has only minor effects on the lifetime artifacts that

occur. The curves generated by eq. 11 differ from the curves of case II only in the value of the slope of $\log[r(t)]$ at long times; the asymptotes of the curves are not horizontal lines but, rather, sloping lines that reflect the additional decay mode.

Fig. 6 shows the $r(t)$ time dependence that results when each component $r_i(t)$ has two correlation times and the internal motion of the fluorophore with the longer lifetime is more restricted than that of the short-lifetime component ($\alpha_2 < \alpha_1$). The lowest curve in fig. 6 is calculated with $\tau_1 = \tau_2$ and therefore contains no heterogeneity distortion. The upper curves are generated using increasing values of τ_2. When τ_2 is only slightly larger than τ_1, the slope of the decay at long times increases but appears to be linear over this time scale. Only when the ratio τ_2/τ_1 is larger than approx. 1.5 are the lifetime heterogeneity effects recognizable. Comparison of fig. 6 with fig. 4c shows the effect of inclusion of overall particle rotation. Comparison of fig. 6 with fig. 3b indicates that nearly identical behavior can be produced by either single-exponential $r_i(t)$ decays with two different particle correlation times or double-exponential decays with rapid but restricted internal motion and the same overall particle rotation time.

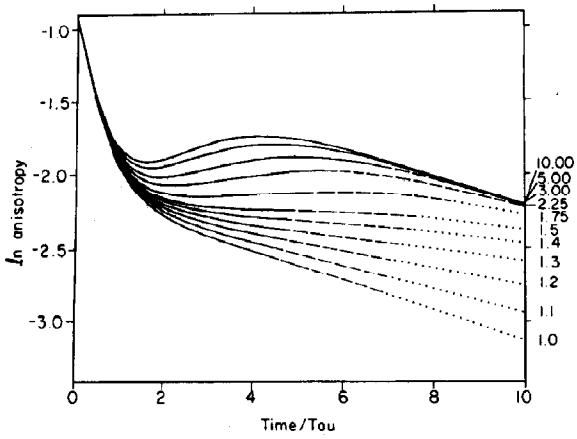

Fig. 6. Simulated anisotropy decays for case III calculated from eq. 11. The curves differ in the value of τ_2, the long lifetime, with $\tau_1 = 1.0$, $a_1 = 0.9$, $\phi_1 = \phi_2 = 0.5$, $\alpha_1 = 0.75$, $\alpha_2 = 0.25$, and $\phi_p = 10$. The values of τ_2 (lower to upper curves) are 1.0, 1.1, 1.2, 1.3, 1.4, 1.5, 1.75, 2.25, 3.0, 5.0 and 10. The lines are drawn as for fig. 2.

The types of $r(t)$ decays that result from eq. 11 are similar in all details to the behavior described above under case II. When $\alpha_2 \neq \alpha_2$, the particle correlation time may be overestimated ($\alpha_1 > \alpha_2$) or underestimated ($\alpha_1 < \alpha_2$). The extreme of overestimation is, of course, the false appearance of decay to a constant, nonzero anisotropy. When $\phi_2 \neq \phi_1$, the particle correlation time may also be overestimated ($\phi_2 > \phi_1$) or underestimated ($\phi_2 < \phi_1$).

4. Discussion

The analysis of anisotropy experiments with inclusion of the possibility of heterogeneity of the fluorophore environments involves several more or less independent questions. On the one hand, it is of interest to see if there are cases of anisotropy decay where a heterogeneous environment mechanism of the type described here is the only possible explanation. If so, the issue becomes the possibility of extracting, without ambiguity, the underlying behavior of the individual environments from the observed anisotropy decay. On the other, there are cases where the anisotropy decay of a heterogeneous population of fluorophores has the same general appearance as that of the rotational diffusion of a homogeneous population of fluorophores with an intrinsic multiplicity of correlation times. It is of interest to compare these two models to see if they can be distinguished. This raises the issue of whether a model based on heterogeneous behavior can be eliminated as an alternative explanation for what appears to be homogeneous behavior with several correlation times.

Some of the anisotropy decay curves of figs. 3–6 have features that clearly suggest heterogeneous behavior. The most obvious of these are those that decrease from a high initial value ($r_0 \approx 0.4$) to a minimum and then rise at longer times. Similarly, those decays that exhibit downward curvature imply a multiplicity of species with distinct motional and excited-state decay behavior. Figs. 1 and 8 show experimental examples of these two cases. Experimental behavior of this type can be explained on the basis of a correlated lifetime and motional distribution and, with some reserva-

tions, this is the only explanation. An interesting comparison can be made with the form of the anisotropy decay for an ellipsoid of revolution [42], which, in some circumstances [43], gives rise to anisotropy behavior that has similar features. In the case of an ellipsoid of revolution the anisotropy is given by a sum of three exponential terms with preexponential factors that depend on the orientation of the absorption and emission dipoles relative to the symmetry axis of the ellipse and the angle between the projection of both vectors on the plane perpendicular to the symmetry axis. For certain cases, one or more of the preexponential factors are negative and thus it is possible to have an anisotropy that increases in time. It is easy to show, however, that if $r(0) = 2/5$ (i.e., the absorption and emission transition dipoles are colinear), then all three preexponential factors are positive and the anisotropy decay for such a case decreases monotonically with upward curvature. This is also the case for a general ellipse. Thus, if $r_0 \approx 0.4$, anisotropy behavior of the kind described above must be due to correlated lifetime and anisotropy heterogeneity.

It is interesting to note that the converse of this argument also applies: if an anisotropy decay exhibits rising behavior following an initial decrease from a high value or shows downward curvature, then the sample must have a heterogeneous lifetime decay even if this is not detected in the direct analysis of the total fluorescence decay.

An example of the rather complex anisotropy time dependence that can result for an ellipsoid of revolution is shown in fig. 7. This case is for a highly elongated prolate ellipsoid with $D_{\|}/D_{\perp} = 30$ and with the absorption and emission dipoles oriented relative to the symmetry axis such that $\cos\theta = 0.3$ ($\theta = 72.5°$) and relative to each other such that the angle between their projections into the x, y-plane is 180° [43]. For this orientation of dipoles, the value of r_0 is 0.203. The resulting time dependence of the anisotropy observed in this case is similar to that presented for heterogeneous behavior in fig. 3, particularly the upper curves of fig. 3b. The anisotropy decay of the ellipsoid shown in fig. 7 was therefore analyzed using a heterogeneous model to see if these two very different physical origins for this type of behavior

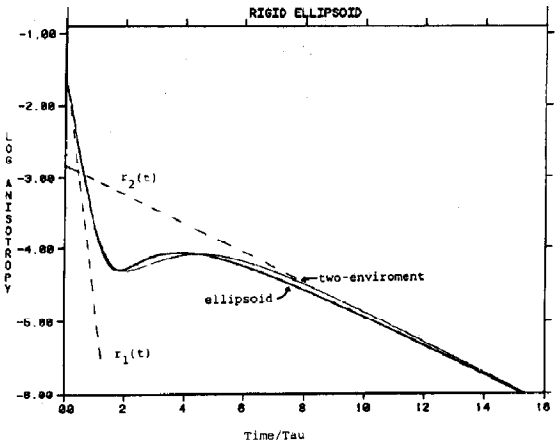

Fig. 7. Anisotropy decay expected for rotational diffusion of a prolate ellipsoid with $D_{\perp} = 1/30$ and $D_{\|} = 1/2$, with the absorption and emission angles oriented relative to the symmetry axis such that $\cos\theta = 0.3$, and with the angle between the projection of the dipoles in the x, y-plane of $\phi = 180°$ [42,43]. For this case $r_0 = 0.2034$. The rotational preexponential factors and correlation times are $r_1 = 0.0533$, $\phi_1 = 5.0$, $r_2 = 0.2484$, $\phi_2 = 0.484$, $r_3 = -0.0983$ and $\phi_3 = 1.5$. The result of a fit to a heterogeneous environment model is also shown. For this fit, the parameters of the fluorescence decay were fixed at $a_1 = 0.9$, $a_2 = 0.1$, $\tau_1 = 1$ and $\tau_2 = 3$. The optimized anisotropy decay for each environment is shown as the dashed straight lines: $r_1 = 0.222$, $\phi_1 = 0.418$, $r_2 = 0.062$ and $\phi_2 = 4.790$. Here the subscripts refer to the lifetime components. Note that the parameters of the two environments of the heterogeneous model are close to two of the components of the motion of the ellipsoid of revolution. The value of r_0 for the heterogeneous model is 0.284, significantly higher than the true value of 0.203.

could be distinguished. For simplicity, the parameters of the fluorescence intensity decay were fixed at $a_1 = 0.9$, $a_2 = 0.1$, $\tau_1 = 1$ and $\tau_2 = 3$. The anisotropy for each environment is represented by a simple exponential decay with an adjustable time constant and initial anisotropy. Optimization of these parameters to fit the 'data' generated from this anisotropy decay as described below results in the fit shown in fig. 7. The resulting χ^2 value for a reasonable count level is 1.2. The details are given in the figure legend. The conclusion is that, if a decay of the type observed in fig. 7 were observed, it might be possible to interpret it in terms of heterogeneous behavior rather than anisotropic rotational diffusion of a single species. This ambiguity exists because of the relatively low value of the initial anisotropy. However, it should be noted

that in order to interpret this ellipsoid anisotropy behavior in terms of a heterogeneous model, it is necessary to use two very different values for the initial anisotropies of the two 'environmental' species. The species with a rapid reorientational motion ($\phi_1 = 0.42$) has a value of r_0 of 0.222 while the species with slow motion ($\phi = 4.8$) has a very low initial anisotropy ($r_0 = 0.062$). These features are necessary in order to obtain the qualitative behavior observed, since the anisotropy only rises slightly before beginning its long-time behavior. Furthermore, the value of the anisotropy at time zero for the heterogeneous model is 0.284 compared to the actual value of 0.222 for this ellipse. If a single chemical species is responsible for the fluorescence, it may be possible to eliminate this interpretation of the anisotropy behavior on spectroscopic grounds. However, it is possible that the low and very different apparent values of the initial anisotropy could be attributed to very rapid motion on a time scale that is too rapid to be resolved in a particular experiment. The proposed motions would have to be of very different amplitudes for the two environments. The degree to which this explanation is reasonable depends on the particular system under study.

The next issue is the extent to which a numerical analysis of anisotropy data exhibiting the kind of behavior described above uniquely determines the true physical parameters of the system. In order to answer this we have used the computations presented above to simulate realistic experimental data. These calculations result in representations of the experimental I_V and I_H transients. These are analyzed simultaneously as described by Cross and Fleming [44] so that the parameters of both the fluorescence decay and the anisotropy for each environment are extracted from the data. In this way any difficulties in the analysis of the total fluorescence decay (due to small amplitudes of one component or closely spaced lifetimes, for example) are propagated into the determination of the anisotropy parameters. The use of an actual instrument response function in the simulations means that the dimensionless variables of the ideal cases become real time in the representation of experiments. (In figs. 3–6 the time scale becomes nanoseconds.) The resulting data sets were analyzed using both 'associated' and 'nonassociated' models, i.e., the actual case where each fluorescence decay lifetime component has a distinct anisotropy decay and the alternative case of a common anisotropy behavior for all components of the sample.

The cases of fig. 3a represent variation in the amplitude of a component with a lifetime of 2 ns and a rotational correlation time of 5 ns relative to another species with a lifetime of 1 ns and a rotational correlation time of 0.5 ns. The limiting curves at the top and bottom correspond to unity and zero for the amplitude of the long-lifetime species; the intermediate curves from the top downward have fractional values of 0.6, 0.35, 0.2, 0.1, 0.05, 0.025 and 0.01. Analysis of these curves yields parameter values in good agreement with the input numbers and χ^2 values ranging from 1.15 (for 60% long lifetime) to 1.3 (1% long lifetime). As expected, the value of the amplitude and lifetime of the long-lifetime component becomes uncertain when this component is present at only a small percentage. The application of a nonassociative single-environment model to these cases results in much larger values of χ^2, nonphysical values of the parameter, or both.

A detailed description of a specific case will illustrate the general nature of the results of these analyses. In fig. 3b the curves represent various values of the ratio of the long lifetime to the short lifetime for a fixed amplitude of the long-lifetime component of 0.1 and rotational correlation times of $\phi_1 = 0.5$ and $\phi_2 = 5.0$ ns for the two species. The initial anisotropy is 0.4 for both components. The fourth curve from the top ($\tau_2 = 1.75$ ns, $\tau_1 = 1.0$ ns) shows clear upward curvature from 2 to 6 ns where a maximum is reached. The intensity of the fluorescence is 0.5% of its initial value at this maximum. The signal-to-noise ratio is about 75 at this point for the simulation used. Analysis of these data yielded the correct parameters of the fluorescence decay: $\tau_1 = 1.003 \pm 0.001$, $\tau_2 = 1.77 \pm 0.01$, $a_1 = 0.906 \pm 0.001$, $a_2 = 0.094 \pm 0.001$. In the heterogeneous model, each of these lifetime components is associated with a distinct environment having an anisotropy decay described by a single exponential plus a constant term. The initial anisotropy for each environment is treated as an

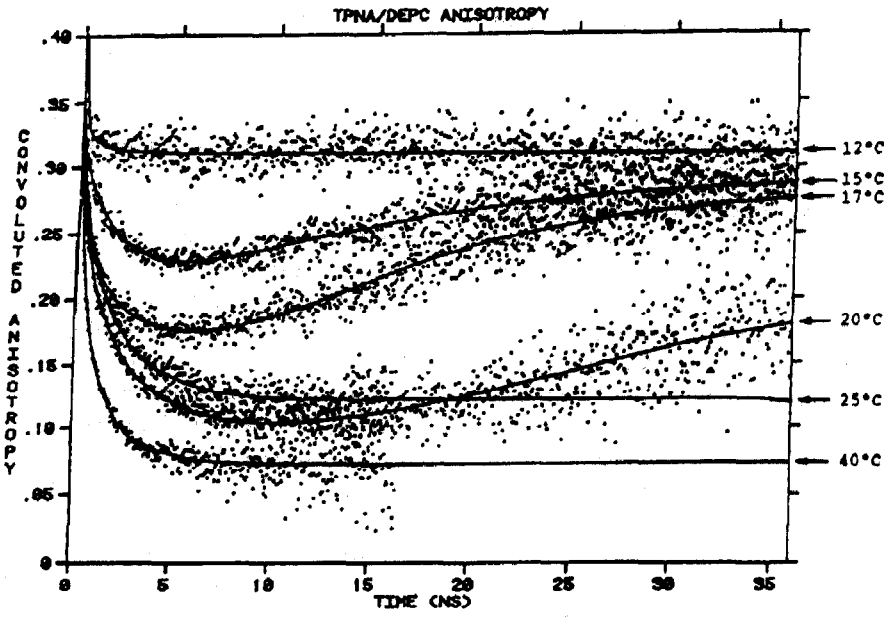

Fig. 8. Anisotropy decay behavior of *trans*-parinaric acid in large unilamellar vesicles composed of dielaidoylphosphatidylcholine. The sample temperature is indicated on the right. The experimental data points are fitted to a general model involving two environments, one 'solid-like' with a high anisotropy and a long average lifetime and one 'fluid-like' with a low anisotropy and a short average lifetime [1,19]. The anisotropy behavior for each environment is described by the model presented in ref. 8.

adjustable parameter. The resulting fit parameters are quite close to the true values: $r_1 = 0.397 \pm 0.001$, $r_2 = 0.386 \pm 0.001$, $\phi_1 = 0.499 \pm 0.001$, $\phi_2 = 4.94 \pm 0.17$, $r_{\infty 1} \approx r_{\infty 2} \approx 0.003$. This gives a value of $\chi^2 = 1.28$.

For this case there is also a local minimum in the χ^2 surface at $\chi^2 = 1.54$ with the same (correct) parameters for the fluorescence decay but in which each environmental anisotropy decays rapidly ($\phi \approx 0.5$ ns) to a constant value ($r_{\infty 1} = 0.048$, $r_{\infty 2} = 0.091$). This is the kind of behavior illustrated in fig. 4a and b and represents the fact that the curves of fig. 4b with a smaller value of $r_{\infty 2}$ are very similar to the intermediate curves of fig. 3b except at times that are so long that the data may not be sufficient to distinguish term.

The alternative analysis of this same simulation in terms of a single environment with double-exponential decay behavior for both the fluorescence intensity and anisotropy decay leads to several minima on the χ^2 surface. In all fits the correct fluorescence lifetimes and amplitudes are recovered. The best fit for this model has $\chi^2 = 1.32$, only slightly higher than the correct analysis ($\chi^2 = 1.28$). The parameters are $\phi_1 = 0.520 \pm 0.006$ (essentially the correct value) and $\phi_2 = 1.39 \pm 0.15$, a relaxation time not corresponding to any actual motion. The amplitudes for the components of $r(t)$ are $r_1 = 0.404 \pm 0.011$, $r_2 = -0.075 \pm 0.010$ and $r_3 = r_\infty = 0.071 \pm 0.010$. The key point is the negative value of r_2 and the finite value of the constant term. These are required to fit the rising behavior of the anisotropy at intermediate times. It is argued above that, given the value of 0.4 for the initial anisotropy, there is no physical model that can result in this type of behavior. It is difficult to reject this fit on statistical grounds, however.

This particular case is of interest in several respects. First, the long lifetime is only 1.75-times the short lifetime and this species is present at a level of only 10%. Thus, this fluorescence decay might very well be misinterpreted as a single-exponential decay. Furthermore, three different

models of similar complexity are roughly equally good statistical fits to the data. As the relative value of τ_2 increases (moving upward in fig. 3b), the alternative solutions for the choices of parameters become statistically or physically less reasonable. Thus, for the case of $\tau_2/\tau_1 = 3.0$ (the second curve of fig. 3b), the 'correct' parameters are recovered with a χ^2 of 1.13 and the alternative heterogeneous solution involving rapid decay of the anisotropy in each environment to constant values has a χ^2 of 9.18. This is due to the fact that this alternative model cannot fit the decrease in $r(t)$ at long times beyond the peak near 5 ns where the total intensity still has a value 2.5% of that of the initial value. The homogeneous model with an anisotropy described by two exponentials plus a constant limiting anisotropy results in a large negative amplitude for the slow correlation decay and a value of $\chi^2 = 6.7$.

It should be noted that the proper interpretation of an anisotropy decay may depend on experimental observation of behavior at short and long times. This may be difficult in some cases. Thus, in the cases of the lower curves of fig. 4a and b, failure to resolve the behavior at short times would result in an anisotropy decay similar to that expected for an anisotropic rotor with a low initial anisotropy.

Fig. 8 shows an experimental example of behavior similar to that shown in fig. 4a and b as well as its analysis [19]. This is a particularly clear case in terms of the unambiguous determination of the parameters. For example, at a temperature of 17°C this sample has 17% of a component with a high limiting anisotropy and a lifetime of 31 ns while the major component with a low limiting anisotropy has an average lifetime of only 4.6 ns. The χ^2 value is 1.12 for the fit to the lifetime data. The initial anisotropies for each component are close to 0.4. As a result, the curve is very similar to the topmost two cases of fig. 4b.

We now turn to the case of behavior for which there is clearly a reasonable explanation in terms of complex motion of a single environment. Thus, those decays that show upward curvature but which do no actually rise at long times can be analyzed, at least qualitatively, in terms of anisotropic rotational diffusion. The question of interest here is whether behavior that appears as anisotropic rotational diffusion can be equally well represented in terms of a heterogeneous model. It should be emphasized that the behavior we are interested in is not dynamic heterogeneity per se, but rather dynamic heterogeneity coupled to excited-state decay heterogeneity. It may be possible to describe a complex anisotropy decay in terms of distinct populations with different motional behavior [15] but if each species in the population has the same excited-state lifetime behavior, the amplitudes and correlation times obtained from a homogeneous model will correspond to real physical motions of at least some of the molecules in the sample if the time scales are well separated or to average values if the correlation times are close together. This is in contrast to the case of heterogeneous lifetime behavior where the time dependence of the anisotropy decay may have no correspondence with any motions of objects in the sample, In this respect, heterogeneous lifetime behavior results in 'artifactual' anisotropy decays.

This emphasizes the importance of careful determination of whether the fluorescence decay of the sample is homogeneous in nature, as would be concluded if it is described by a single exponential, or heterogeneous, a possible explanation for nonexponential behavior. Clearly, if the sample fluorescence contains significant amplitudes of components with widely different lifetimes, this will be detected and the possibility of distinct dynamics for the components will be considered. For this reason we have placed emphasis on those cases where the component lifetimes are rather close together ($\tau_2/\tau_1 < 2$) and the amplitude of one of the components is small (e.g., 10%). This makes the analysis of the fluorescence decay problematical under most experimental conditions. The analysis presented here suggests that this limitation can have a serious influence on the extracted motional parameters.

A specific case illustrating this type of behavior is that of fig. 3b with $\tau_2/\tau_1 = 1.2$ and the amplitude of the 'long'-lifetime component being only 10%. As expected, all analyses have difficulty in extracting the proper amplitudes and lifetimes for the total decay. The lowest χ^2 solutions give $a_1 = 0.91–0.93 \pm 0.03$ with values of τ_1 of 1.01–1.02

and 1.2–1.4 ± 0.06 ns. A two-component model with a value of χ^2 of 1.396 resulted in reasonable parameter values ($r_1 = 0.388$, $r_2 = 0.400$, $\phi_1 = 0.499 \pm 0.002$ and $\phi_2 = 4.295 \pm 1.207$ vs. 5.00 input for this case). Other fits using this two-component model resulted in two equal correlation times of 0.5 ns and finite positive and negative limiting anisotropies for the two species. The χ^2 values for these fits were exactly the same as that for the correct fit with zero limiting anisotropies. Thus, there is an ambiguity in the analysis of this type of data even within the context of the correct model unless there is a physical basis for rejecting the case of a finite limiting anisotropy.

Analysis of the same data under the assumption that all of the species in the sample have the same motional behavior results in an equally good fit to the data ($\chi^2 = 1.396$) and results in reasonable parameter values: $r_1 = 0.359$, $r_2 = 0.027$, $\phi_1 = 0.495 \pm 0.002$ and $\phi_2 = 10.698 \pm 10.730$. Note that the value of ϕ_2 is consistent with inspection of the curve in fig. 3b. The only clue that this is an incorrect model is the very large (100%) estimated uncertainty in this parameter. We conclude that even in this case of 'minor' heterogeneity in the sample fluorescence, one might deduce anisotropy parameters that differ considerably from the true value.

Perhaps a better example of this is that of the lower curves of fig. 4c. These all correspond to the case of a long-lifetime species with a lifetime of 2 ns and a low limiting anisotropy (0.1) in the presence of a 1 ns species with a high limiting anisotropy (0.3). The anisotropy decay is very rapid for both species ($\phi = 0.5$ ns). The third curve from the bottom corresponds to 60% of the 2 ns component. Analysis with the correct heterogeneous model yields the correct parameters with high precision and small uncertainty. The χ^2 value is 1.145. the homogeneous model results in a χ^2 value of 1.148 with unambiguous (but incorrect) parameter values of $\phi_1 = 0.515 \pm 0.004$ and $\phi_2 = 2.418 \pm 0.077$ and a limiting anisotropy of 0.10. Thus, the lifetime heterogeneity introduces a new correlation time not present in either environment and ignores the 40% of the sample that is highly motionally restricted. It might be argued that in this case the heterogeneity of the sample will be obvious from the analysis of the fluorescence decay. What is found is that analysis of the total decay with a two-exponential decay yields the correct values of the parameters with a χ^2 value of 1.10 while a single-exponential fit to the same data yields an average lifetime of 1.6 ns and $\chi^2 = 1.25$. Thus, a detailed analysis using more sophisticated statistical methods might reveal this heterogeneity. Our results indicate that such an analysis may be warranted to ensure that the correct motional parameters are extracted.

Acknowledgements

This work was supported by NIH grants GM26536 (to B.H.) and training grant GM07759 (R.L.). Preliminary accounts of this work were presented at the 28th Annual Meeting of the Biophysical Society, San Antonio, TX (Biophys. J. 45 (1984) 379a) and the 31st Annual Meeting of the Biophysical Society, New Orleans, LA (Biophys. J. 51 (1987) 285a).

References

1 B. Hudson, D.L. Harris, R.D. Ludescher, A. Ruggiero, A. Cooney-Freed and S.A. Cavalier, in: Fluorescence in the biological sciences, eds. D.L. Taylor, A.S. Waggoner, F. Lanni, R.F. Murphy and R. Birge (Alan R. Liss, New York, 1986) p. 159.
2 M.D. Barkley and B.H. Zimm, J. Chem. Phys. 70 (1979) 2991.
3 J.M. Schurr, Chem. Phys. 84 (1984) 71.
4 K. Kinosita, S. Kawato and A. Ikegami, Biophys. J. 20 (1977) 289.
5 M.P. Heyn, FEBS Lett. 108 (1979) 359.
6 F. Jahnig, Proc. Natl. Acad. Sci. U.S.A. 76 (1979) 6361.
7 P.K. Wolber and B.S. Hudson, Biophys. J. 37 (1982) 253.
8 W. van der Meer, H. Pottel, W. Herreman, M. Ameloot, H. Hendrickx and H. Schroeder, Biophys. J. 46 (1984) 515.
9 G. Lipari and A. Szabo, Biophys. J. 30 (1980) 489.
10 A. Szabo J. Chem. Phys. 81 (1984) 150.
11 T. Ichiye and M. Karplus, Biochemistry 22 (1983) 2884.
12 R.M. Levy and A. Szabo, J. Am. Chem. Soc. 104 (1982) 2073.
13 B. Hudson, R.D. Ludescher, A. Ruggiero, D.L. Harris and I. Johnson, Comments Mol. Cell. Biophys. 4 (1987) 171.
14 J.R. Lakowicz, Principles of fluorescence spectroscopy (Plenum Press, New York, 1983) p. 149, 163.
15 R.E. Dale, L.A. Chen and L. Brand, J. Biol. Chem. 252 (1977) 7500.

16 F. Claesens and R. Rigler, Eur. Biophys. J. 13 (1986) 331.
17 E.R. Rigler and H.E. Ehrenberg, Q. Rev. Biophys. 6 (1973) 139.
18 R.D. Ludescher, Nanosecond dynamics in proteins and lipids: a time-resolved fluorescence anisotropy study, Ph.D. dissertation, University of Oregon (1984).
19 A.J. Ruggiero, Time-resolved fluorescence studies of pretransitional phenomena in phospholipid bilayers, Ph.D. dissertation, University of Oregon (1986).
20 R.H. Austin, S.S. Chan and T.M. Jovin, Proc. Natl. Acad. Sci. U.S.A. 76 (1979) 5650.
21 M.M.S. Lo, P.B Garland, J. Lamprecht and E.A. Barnard, FEB Lett. 111 (1980) 407.
22 R. Zidovetzki, Y. Yarden, J. Schlessinger and T.M. Jovin, Proc. Natl. Acad. Sci. U.S.A. 78 (1981) 6981.
23 M. Bartholdi, F.J. Barrantes and T.M. Jovin, Eur. J. Biochem. 120 (1981) 389.
24 J. Gallay, M. Vincent and A. Alfsen, J. Biol. Chem. 257 (1982) 4038.
25 T. Tao, Biopolymers 8 (1969) 609.
26 A. Grinvald and I.Z. Steinberg, Biochim. Biophys. Acta 427 (1976) 663.
27 I. Weinryb and R.F. Steiner, in: Excited states of proteins and nucleic acids, eds. R.F. Steiner and I. Weinryb (Plenum Press, New York, 1971) p. 277.
28 D. Creed, Photochem. Photobiol. 39 (1984) 537.
29 R.D. Ludescher, J.J. Volwerk, G.H. de Haas and B. Hudson, Biochemistry 24 (1985) 7240.
30 M.C. Chang, J.W. Petrich, D.P. McDonald and G.R. Fleming, J. Am. Chem. Soc. 105 (1983) 3819.
31 J.W. Petrich, M.C. Chang, D.B. McDonald and G.R. Fleming, J. Am. Chem. Soc. 105 (1983) 3824.
32 A.G. Szabo, T.M. Stepanik, D.M. Wayner and N.M. Young, Biophys. J. 41 (1983) 233.
33 J.B.A. Ross, K.W. Rousslang and L. Brand, Biochemistry 20 (1981) 4361.
34 D.R. James and W.R. Ware, Chem. Phys. Lett. 126 (1986) 7.
35 L. Brand and J.R. Gohlke, J. Biol. Chem. 246 (1971) 2317.
36 R.P. De Toma, J.H. Easter and L. Brand, J. Am. Chem. Soc. 98 (1976) 5001.
37 J.R. Lakowicz and H. Cherek, J. Biol. Chem. 255 (1980) 831.
38 J.R. Lakowicz, Biophys. Chem. 19 (1984) 13.
39 E.W. Small and I. Isenberg, Biopolymers 16 (1977) 1907.
40 B. Hudson and S.A. Cavalier, in: Spectroscopic membrane probes, ed. L. Loew (CRC Press, Boca Raton, 1987) in the press.
41 P.K. Wolber and B. Hudson, Biochemistry 20 (1981) 2800.
42 M.D. Barkley, A.A. Kowalczyk and L. Brand, J. Chem. Phys. 75 (1981) 3581 and references therein.
43 L. Brand, J.R. Knudson, L. Davenport, J.M. Beecham, R.E. Dale, D.G. Walbridge and A.A. Kowalczyk in: Spectroscopy and the dynamics of molecular biological systems, eds. P.M. Bayley and R.E. Dale (Academic Press, London, 1985) p. 259.
44 A.J. Cross and G.R. Fleming, Biophys. J. 46 (1984) 45.
45 P.V. Bevington, Data reduction and error analysis for the physical sciences (McGraw-Hill, New York, 1969).